Desalination and Water Treatment
www.deswater.com

doi: 10.5004/dwt.2017.21252

86 (2017) 183–190
August

Investigating the governing decolorization mechanisms of nanodiamond in the treatment of an azo dye

Erick Butler[a,*], Emily Hunt[a], Yen-Pei Fu[b], Oliver Mulamba[a], Noel Spaar[a]

[a]*School of Engineering, Computer Science, and Mathematics, West Texas A&M University, Canyon, Texas, USA, emails: erick.ben.butler@gmail.com (E. Butler), ehunt@wtamu.edu (E. Hunt), omulamba@wtamu.edu (O. Mulamba), noelspaarlives@gmail.com (N. Spaar)*
[b]*Department of Materials Science and Engineering, National Dong-Hwa University, Shou-Feng, Hualien, Taiwan, email: ypfu@mail.ndhu.edu.tw (Y.-P. Fu)*

Received 26 May 2017; Accepted 22 July 2017

ABSTRACT

Heterogeneous photocatalysis is accepted as an efficient method of degrading a wide array of pollutants and inactivating bacteria. Titanium dioxide, the catalyst of choice, is very limited in its applications because of its high-energy band gap and many researchers have opted to employ doping TiO_2 to reduce the band gap between conduction and valence bands. A lot of success stories have been documented where carbon-doped TiO_2 showed improved efficiency as a result, yet no work has attempted to gauge the governing path of treatment that comes with a carbon-based material, and its photocatalytic efficiency. This study assesses the viability of photocatalytic decolorization of acid blue–stained wastewater, using nanodiamond. The findings allow for an understanding of the routes of decolorization governing this carbon-based catalyst and validation of their use as TiO_2 photocatalytic dopants. Decolorization was assessed using three catalysts namely, TiO_2, Fe–TiO_2, and nanodiamond. Feasibility was tested under two different excitation light sources and one set of tests was performed in the dark to negate any photoactivation. In addition, UV–Vis spectra, X-ray powder diffraction and scanning electron microscopy were used to characterize the materials prior to treatment and post-decolorization. Nanodiamond outperformed TiO_2 and Fe–TiO_2 in regards to removal efficiency, rate of removal and breadth of effect. Photocatalysis degradation from nanodiamond samples was confirmed, yet its effects were slight and only observable at the smallest catalyst loading. Nanodiamond exhibited decolorization in both light reactors and in the dark, equally efficiently, while TiO_2 and Fe–TiO_2 showed no life in the dark. These observations are of importance to the aquatic sector that needs to gain good fundamental understanding of the governing parameters effecting treatment efficiency and how to improve them.

Keywords: Photocatalysis; Titanium dioxide; Nanodiamond; Acid Blue 113; Wastewater treatment

1. Introduction

The last two decades has seen growth in interest and research for environmental applications of heterogeneous photocatalytic processes [1–3]. Photocatalysis treatment has been documented to be an efficient method to degrade a wide array of pollutants, in addition to also showing feasibility of inactivating microorganisms including viruses, bacteria, and fungi [4,5]. Heterogeneous photocatalysis is a photochemical treatment process that mineralizes pollutants by using the combination of a semiconductor and a light source. The technology was established in 1972 when Fujishima and Honda split water into ions by the use of the semiconductor titanium dioxide (TiO_2) [6]. Since then, it has been popularized in numerous avenues such as a method of wastewater treatment, particularly the decolorization of dyes. Ibhadon

* Corresponding author.

and Fitzpatrick [7] describe photocatalysis in the following manner. First, pollutants move to the surface of the catalyst. Upon reaching the surface, pollutants are adsorbed onto the catalyst. Once adsorbed, pollutants react on the surface of the photocatalyst. Researchers use sunlight, visible, or ultraviolet (UV) light to initiate these reactions. When a catalyst comes into contact with the light source, excited electrons move from the valence to conduction band in the catalyst. This leaves a positive hole in the valence band. The electron and hole participate in oxidation–reduction reactions forming hydroxyl radicals and superoxide ions [7]. The holes combine with molecules of water to generate hydroxyl radicals, while the electrons interact with oxygen to inevitably form superoxide ions such as peroxide [8]. These charged ions drive the degradation of pollutant dyes into non-inert forms. These non-inert products are then released from the catalyst surface [7].

While titanium dioxide was initially used for splitting water, it has become one of the most common catalysts present in research. This is because titanium dioxide is inexpensive, very photoactive, and low in toxicity. Nevertheless, titanium dioxide is very limited in its applications because of its high-energy band gap (3.2 eV) or the amount of energy necessary to move electron and holes to the catalyst surface. In order to initiate photocatalysis, one will require high energy, usually energy values less than or equal to 387 nm (UV light) [9]. As an alternative, many researchers have opted to employ doping or the process of augmenting titanium dioxide with more energy levels to reduce the band gap between conduction and valence bands. Effective metallic doping occurs at the surface of the photocatalyst. Band gap reduction allows for the absorption of energy within the visible region (400–700 nm) [8]. Materials for doping have ranged from non-metal such as carbon, fluoride, and sulfur, to metallic such as iron, cobalt, and chromium. While doping does, in some cases, prevent the formation of chemical reaction barriers and charge selectivity, there are still numerous concerning issues with doping. Some authors have found that doping could lead to recombination or the formation of electron–hole pairs, preventing the movement of electrons from the valence to the conduction band, and prohibit effective photocatalytic activity [10].

Of the dopants used, carbon-based dopants have been documented as being highly effective in improving the visible-light photoactivity of TiO_2 and to improve the observations of dopants like nitrogen [11–13]. The methods of doping TiO_2 with carbon are many and include sol–gel synthesis, physical and chemical vapor deposition techniques, mixing of carbon-based nanomaterial, hydrothermal synthesis, and direct oxidation of titanium in a burner [14–16]. All these methods, while inducing slight differences in the specifics, all presented data that agreed in regards to the improved photoactivity of the catalyst. In addition, there have been studies that have used carbon-based materials as photocatalysts to treat pollutants [17–19]. Nevertheless, missing from the literature is to determine whether nanocarbon allotropes such as nanodiamond are capable of being effective as photocatalysts. To the author's knowledge, there has been only one study published using nanodiamond to treat dyes but the researcher examined the adsorption behavior of nanodiamond and not its capabilities as a photocatalyst [20].

As such, the main objective of this work is to assess the viability of photocatalytic removal of acid blue dye using nanodiamond to deepen the understanding of the governing routes of removal and carbon-based dopants. To better comprehend observations and deductions, the well-researched and documented photocatalyst TiO_2 and a TiO_2 dopant will undergo mirror experimentations to observe similarities and lack thereof between the removal mediums. This study will provide a good base for quantifying the benefits of carbon-based doping technologies to the water treatment industry.

2. Materials and methods

2.1. Experimental materials and methods

The experiments were conducted using synthetic wastewater. Prior to each run, 100 mL of Acid Blue 113 (Santa Cruz Biotechnology, CA, USA; Fig. 1) stock solution was poured into a 250 mL beaker. Catalysts were measured and added to the beaker prior to the run. The beakers were placed inside of the reactor and covered with watch glass to minimize the loss of solution by evaporation during irradiation time.

Pure titanium dioxide (TiO_2) and 2 mol% ferric-doped titanium dioxide (Fe–TiO_2) nanopowders were the designated titanium dioxide photocatalysts in this study. Synthesis of pure titanium dioxide was prepared by sol–gel hydrolysis precipitation [21]. Procedures for the synthesis of 2 mol% ferric-doped titanium dioxide (Fe–TiO_2) can be found in reference [22]. Nanodiamond (95% purity, 3–4 nm; SkySpring Nanomaterials Inc., Houston, TX, USA) powders were used in this study. Three identical 30-qt aluminum, enclosed cylindrical reactors were used to conduct the experiments. The reactors were housed side-by-side in a closed, dark room to avoid photocatalyst contact with ambient light. Each reactor was assigned a light source. This was done to minimize error when exchanging light sources among reactors. Two light sources were used—a 160-W mercury vapor UVB in the range of 200–800 nm and a xenon high intensity discharge (HID) lamp (6,000 K). The third reactor was to conduct experiments without light. The catalyst loading range was from 0.025 g to 0.1 g per 100 mL of wastewater sample. Prior to the contact with a light source, the beakers are stirred in the dark for 20 min to ensure a homogenous mixture and maintained equilibrium throughout the sample. Following the stirring,

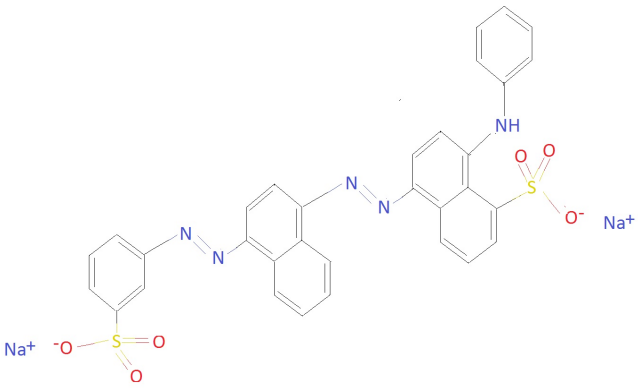

Fig. 1. Chemical structure of Acid Blue 113.

the light source is turned on and an aliquot of sample is collected after 30, 90, and 150 min of contact with the light source.

2.2. Sample analysis

2.2.1. Wastewater analysis

The samples are centrifuged at 3,900 rpm for 1 h (Sigma 2-6E Centrifuge, Sigma Laborzentrifugen, Germany). The purpose was to ensure that there was adequate separation between wastewater and the photocatalyst. After centrifugation, the supernatant of the sample is extracted and read by a UV–Vis spectrophotometer (Hach DR6000 UV–Vis spectrophotometer with RFID Technology, Hach, USA). A wavelength scan (200–900 nm) is completed on each sample. This is done three times and averaged. The results are expressed using the peak wavelength from the scan (565 nm). Dye removal by decolorization is calculated by the following equation:

$$\text{Decolorization}\ (\%) = \left(\frac{C - C_o}{C_o}\right) \times 100 \quad (1)$$

where C is the concentration at any time t (mg/L); C_o is the initial concentration (mg/L).

2.2.2. Materials characterization

X-ray powder diffraction (XRD) patterns were recorded on a Rigaku Smartlab XRD system. The patterns were used to assess potential structural changes in the catalysts before and after treatment. The scanning electron microscopy (SEM) images collected on a JEOL JSM7100 were used to observe whether there were any morphological changes taking place in the catalyst after treatment as compared with before. After wastewater analysis, samples for each catalyst observed to show highest decolorization removal were processed and prepared for post-treatment assessment. The preparation process is as follows: after 180 min of irradiation time, the entire beaker contents were placed into an evaporation dish. Prior to the content placement, the evaporation dish had been washed, dried in an oven (Lab Companion AAH14016U Economy Mechanical Convection Oven; 115 VAC) at 180°C ± 1°C (temperature control accuracy) for 1 h and cooled. After content placement, the dish was placed back into the oven at 180°C ± 1°C for about 4½ h. This was done to evaporate the liquid and the leave solid material behind. The dishes were then cooled, covered, and placed into a fume hood until analysis was performed.

3. Results and discussion

3.1. Effects of light source on Acid Blue 113 removal

3.1.1. Removal by TiO_2 and Fe–TiO_2

Figs. 2(a) and (b) summarize the removal of Acid Blue 113 based on the type of catalyst employed. It is observed that treatment efficiency is predicated on the type of light source. These results are comparable with what is found in the literature [23–25]. Under dark conditions, there was very little treatment found when using Fe-doped TiO_2 or pure titanium dioxide. Treatment ranged between −2.03% and +2.41% for Fe-doped TiO_2 and −1.55% and +1.41% for titanium dioxide. The lack of efficiency in the dark indicates that decolorization of Acid Blue 113 occurs because of photocatalysis and not adsorption [26]. When using a light source, it was observed that treatment efficiency improved when using UVB illumination as compared with the HID lamp.

UVB illumination showed a significant improvement in treatment efficiency as compared with the HID xenon lamp for both the TiO_2 and Fe–TiO_2. Results show improved decolorization efficiency with TiO_2 as compared with Fe–TiO_2 regardless of light source. The catalysts performed more efficiently in UVB illumination as compared with the xenon HID lamp. This is because of the fact that UVB illumination occurred in the range of 200–800 nm that would be sufficient energy for the photocatalysis by TiO_2. A potential reason why TiO_2 had higher decolorization of Acid Blue 113 as compared with Fe–TiO_2 is because of the doping of TiO_2 with transition metals. At times, the doping of TiO_2 may be the catalyst for recombination or limit available reaction sites on the catalyst surface [10]. Calculations show that this drop of efficiency lies somewhere between 5.66% and 7.58% less decolorization. Also observed is the decolorization efficiency as a result of catalyst loading for each catalyst. In general, it has been observed that as the catalyst loading increases, dye decolorization increases, which

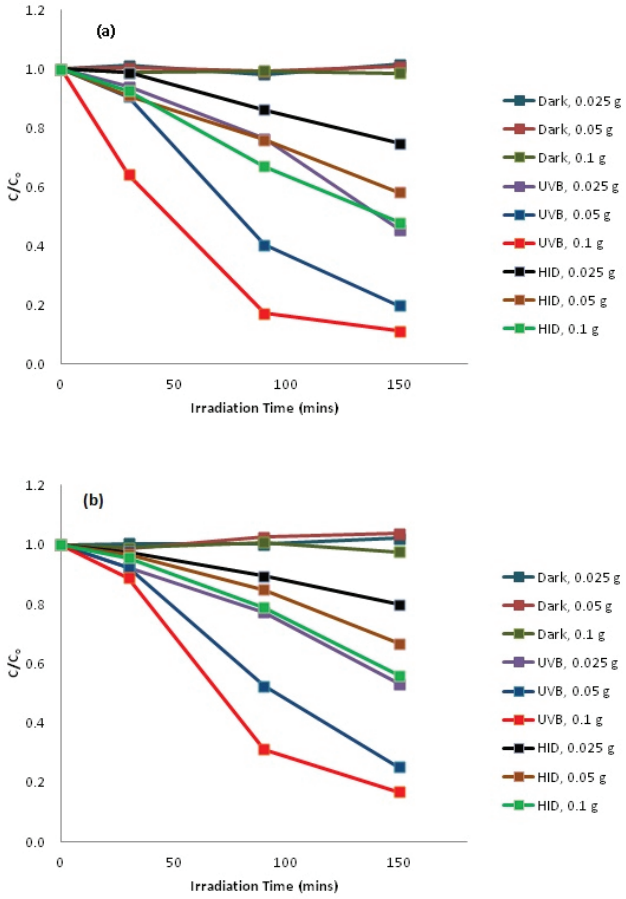

Fig. 2. Effects of catalyst loading on the removal of Acid Blue 113 over irradiation time by (a) TiO_2 and (b) Fe–TiO_2 at a wavelength of 565 nm.

is the case here. This has been attributed to an increase of both the total active surface area and the available active sites on the catalyst [27]. However, several studies have demonstrated that there is a limit on the amount of catalyst for efficient treatment. The maximum catalyst loading reported by several authors for effective treatment has been 0.1 g/100 mL or 1 g/L [26, 28,29]. However, when the catalyst loading reaches a value greater than 0.1 g/100 mL, turbidity within the reactor increases. Turbidity not only decreases the volume of catalysts, but it also prevents the light source from passing through. As a result, photocatalytic activity decreases [27].

3.1.2. Removal by nanodiamond

According to the results summarized in Fig. 3, nanodiamond removed 81%–100% under dark conditions, 80.47% to 99.9% under UVB illumination, and 79.26%–100% using HID as a light source. It is observed that at the low loading concentration of 0.025 g, the change in light source results in a change in the decolorization. Treatment by UVB illumination is the most efficient, followed by treatment by the HID lamp. Treatment under dark conditions is the least efficient. The rates of removal, even at low loading, are substantially greater than what is seen in the cases of TiO_2 and Fe–TiO_2 results. The effect of the light source appears negated when an increase in catalyst loading takes place. The loading change is found to substantially increase the decolorization of Acid Blue 113, while the type of lighting no longer appears to enhance one over the other. The rate of decolorization appears to be increased with loading increases, reaching a higher amount of treatment in as short of a testing time.

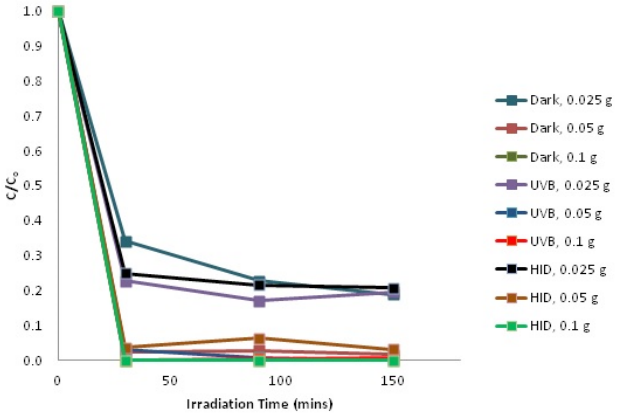

Fig. 3. Effects of catalyst loading on the removal of Acid Blue 113 over irradiation time by nandiamond at a wavelength of 565 nm.

3.2. UV–Vis spectra analysis

UV–Vis spectra graphs (200–800 nm) for the degradation of Acid Blue 113 by Fe–TiO_2, pure TiO_2, and nanodiamond have been developed. Figs. 4(a)–(f) provide UV–Vis spectra for TiO_2, Fe–TiO_2, and nanodiamond using the HID xenon lamp. The UV–Vis spectra graphs demonstrate a change in absorbance over irradiation time. The graphs also present two peaks at the initial time (t = 0)—565 nm (visible region) and the other at 275 nm (UV region). The primary peak used to analyze the results from the experiments was the 565 nm peak. From these spectra, we observe that absorbance at the visible region decreases as time elapses for Fe–TiO_2, pure TiO_2, and nanodiamond, even though the rate of decrease is greater in the latter.

The primary peak used to analyze the results from the experiments was the 565 nm peak. From these spectra, we observe that absorbance at the visible region decreases as time elapses for Fe–TiO_2, pure TiO_2, and nanodiamond.

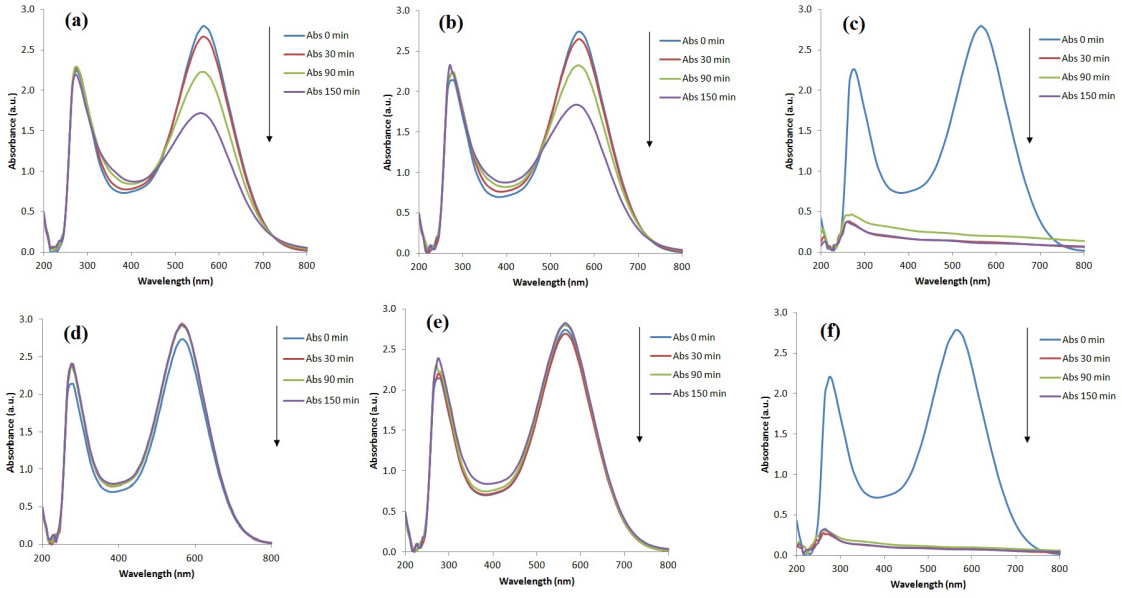

Fig. 4. UV–Vis spectra (200–800 nm)—(a) 0.05 g TiO_2 using HID xenon lamp; (b) 0.05 g Fe–TiO_2 using HID xenon lamp; (c) 0.05 g ND using HID xenon lamp; (d) 0.05 g TiO_2 under dark conditions; (e) 0.05 g Fe–TiO_2 under dark conditions; (f) 0.05 g ND under dark conditions.

The graphs confirm patterns of degradation for all three catalysts under irradiation. The nanodiamond behavior stands alone as it shows a decrease in both the 565 nm peak and the 275 nm UV region peak. This indicates that the treatment of the wastewater using the nanodiamond is not merely decolorization. When similar experiments are performed under dark conditions, there are no patterns of degradation shown by Fe–TiO_2 and pure TiO_2. On the other hand, nanodiamond appears to have similar effects in the dark as it has in the light. Figs. 3(d)–(f) show the UV–Vis data for experimentation performed in the dark. The UV–Vis spectrum for nanodiamond under dark conditions shows efficient degradation of Acid Blue 113. In the UV region, there is a difference in the trend between the peaks under dark and light conditions. For Fe–TiO_2 and TiO_2, the trend witnessed in these graphs is that under dark conditions, the peak increases over irradiation time. However, absorbance peaks at 2.393 after 150 min of irradiation when using Fe–TiO_2 as the catalyst. The trend for TiO_2 indicates that as the irradiation time increases, the absorbance increases as the peak maximizes at 2.407 after 150 min. This pattern is similar to the one observed using Fe–TiO_2. The peaks in the UV region for nanodiamond show a major decrease in absorption after 30 min for both dark and light conditions—the peaks increase from 30 to 90 min, and decrease from 90 to 150 min. The patterns are identical not only to the pattern of behavior for visible light but also for the UV and visible light peaks. One possible explanation is the formation of intermediates from the degradation of Acid Blue 113 [30]. Because Acid Blue 113 is an azo dye, the resulting degradation products include CO_2, NH_4^+, NO_3^-, Cl^-, and SO_4^{2-} [31,32].

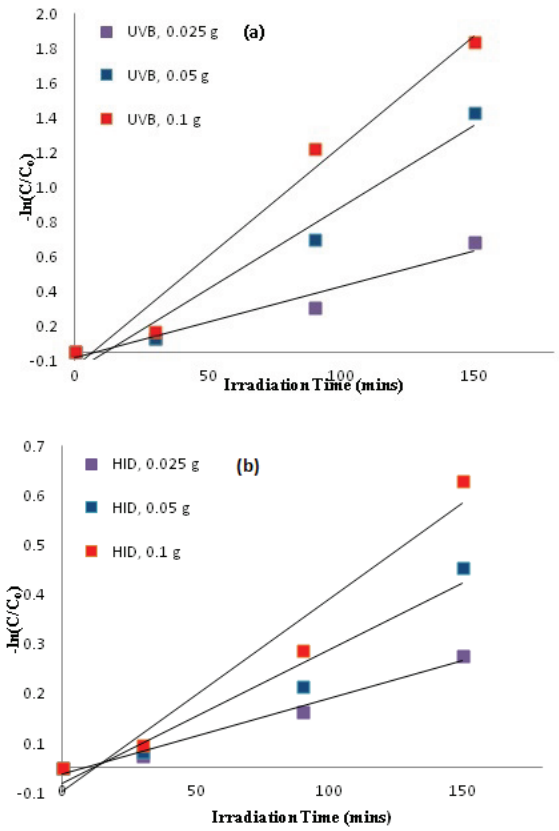

Fig. 5. The determination of kinetic behavior within the experiment using UVB illumination for (a) Fe-doped TiO_2 and (b) TiO_2.

3.3. Kinetic relationships

One of the best predictors of treatment efficiency is to determine the kinetic relationship. In most cases, treatment by photocatalysis typically follows first-order kinetics [22,33,34] expressed by the following:

$$\ln\left(\frac{C}{C_o}\right) = -k_{\exp}t \tag{2}$$

where C is the concentration at any time t (mg/L); C_o is the initial concentration (mg/L); k_{exp} = experimental kinetic rate constant (min^{-1}); t = treatment time (min).

To compute the kinetic rate constant and confirm a first-order rate, $-\ln(C/C_o)$ vs. irradiation time was plotted for each experimental condition (Figs. 5(a) and (b)). Please note that since samples in the dark did not produce any significant results, they were not included in this discussion. In addition, nanodiamond catalysts were not included in the analysis since significant removal occurred at an accelerated rate within the first 30 min of irradiation. According to the results, the experimental kinetic rate increases with increasing catalyst loading for all conditions. For Fe-doped TiO_2, the kinetic rate constant increased from 0.0041 to 0.0127 min^{-1} as compared with the kinetic rate constant 0.0015 to 0.0039 min^{-1}. Degradation was 2.7 to 3.3 times higher for those experiments under UVB illumination as compared with HID.

On the other hand, the kinetic rate constant for pure TiO_2 increased from 0.0052 to 0.0153 min^{-1} under UVB illumination, while HID increased from 0.002 to 0.005 min^{-1}. These results indicate that degradation was 2.6 to 3.1 times for UVB illumination as compared with experiments using HID. Overall, the R^2 values for pure TiO_2 are greater than 0.92, while the R^2 value for Fe-doped TiO_2 are greater than 0.95. The R^2 values indicate that it is reasonable to use first-order kinetics to describe the pattern of behavior witnessed within these results.

3.4. The effects of light source on the degradation behavior of nanodiamond

Garg et al. [35] explain that the purpose of stirring a sample in the dark is to determine whether photocatalysis or adsorption is responsible for the decolorization of the dye wastewater. For all experiments with the exception of those using nanodiamond compile little or no color removal when stirring the samples in the dark. These values confirm that treatment efficiency was primarily photocatalysis. On the other hand, experimental runs that use nanodiamond result in similar color removal efficiencies between light and dark conditions. The results under dark conditions confirm the work of Wang et al. [20] which found adsorption as a mechanism by which an azo dye is removed. As previously mentioned, the photocatalyst capabilities of nanodiamond had not been studied prior to this work. Therefore, the results under light conditions have rendered an opportunity to study the behavior of nanodiamond as a photocatalyst in the future.

In addition, experiments that involve nanodiamond using the HID lamp and under UVB irradiation appear to exhibit behavior that is quite different from what is seen with TiO_2 and Fe–TiO_2 under those same conditions. Referring back to Fig. 2, there appears to be an immediate reduction in the (C/C_o) ratio after a sample is collected after 30 min of irradiation time. A potential reason behind this could be adsorption occurring during the initial 20 min of stirring. If one compares the samples involving under dark conditions with those under the light, this pattern of behavior is present. However, samples that are irradiated for 30 min appear to have a much lower (C/C_o) ratio as compared with those that simply remain in the dark after initial stirring. The mechanisms that appear to be involved include photocatalysis and adsorption. The significance of this pattern of behavior is that it would greatly reduce the treatment time to 30 min of irradiation as opposed to at the minimum of 2–3 h.

However, does this hold true when analyzing color removal between experiments in the dark and those in the light after the 30 min of irradiation? The results indicate that the improvement of color removal is contingent on the catalyst loading. At 0.025 g of nanodiamond, adsorption and photocatalysis improve treatment from 65.81% (adsorption only) to 75.08% (HID) and 77.33% (UVB), an increase in color removal between 14.1% and 17.5%. However, when the catalyst loading increases, the use of adsorption and photocatalysis does not enhance treatment. In fact, it decreases at 0.05 g and is about the same at 0.1 g. Nevertheless, the results from this experiment could demonstrate that nanodiamond is not only capable of removing wastewater under irradiation and in the dark, it could also lead to research using a smaller dose of a catalyst in order to achieve a valuable result. Compared with joint results, nanodiamond is viable to decolorize dye wastewater on its own.

3.5. Material characterizations

3.5.1. XRD analysis

The XRD data (Fig. 6) shows overlay comparisons of the pre- and post-decolorization structures. The TiO_2 and Fe–TiO_2 structures do not show any noticeable changes during the transition. It is observed that there is indeed a change in the post-nanodiamond sample, seen as an increase in peak intensity and width, and the manifestation of two peaks that relate to acid blue (shown with down pointing arrows). Literature states a number of potential reasons for increase in full-width at half-maximum, some of which are inhomogeneous composition, microstrain and other defects in the crystal structure. The Halder–Wagner method provided on the PDXL Rigaku software was used to assess the potential reasons for the observed changes in structure. In the Halder–Wagner method, size and strain effects are correlated to the integral breadth components described by the Lorentzian and Gaussian functions.

The strain and crystallite sizes were calculated using the following equation:

$$\left(\frac{\beta\cos\theta}{\sin\theta}\right)^2 = \frac{K\lambda}{D}\times\frac{\beta}{\tan\theta\sin\theta}+16\varepsilon^2 \quad (3)$$

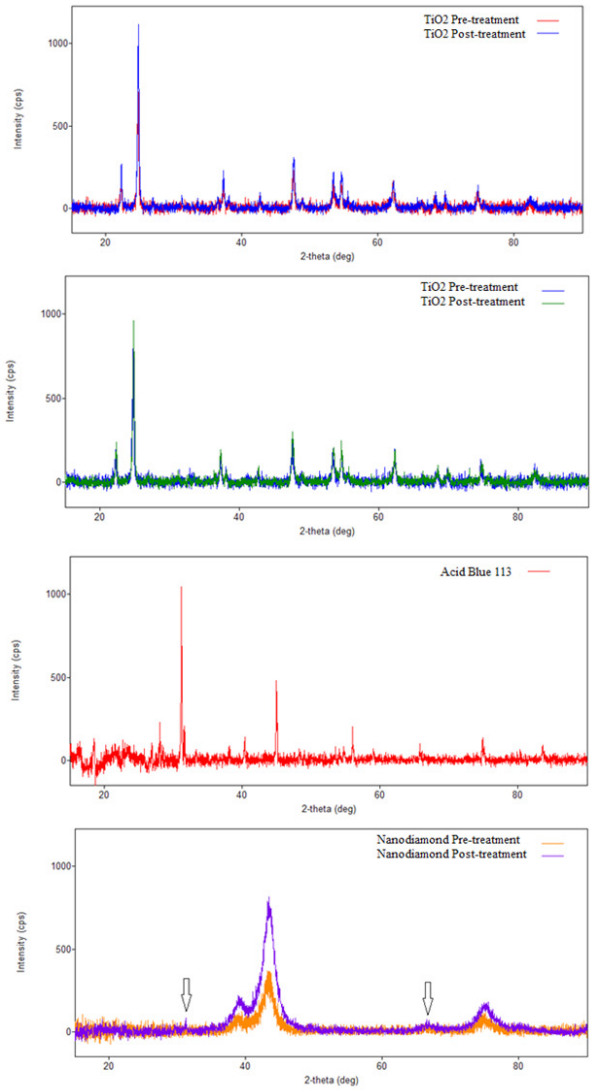

Fig. 6. XRD comparison between pre- and post-treatment for TiO_2, Fe–TiO_2, acid blue, and nanodiamond.

where both the microstrains and small crystallite sizes are tied to the integral breadth β, λ is the wavelength of Cu Kα radiation, D is the crystallite size, K is the Scherrer constant depending on the crystallite configuration, and ε is the weighted average strain. When we plot $(\beta/\tan\theta)^2$ against $\beta/(\tan\theta\cdot\sin\theta)$, the y-intercept gives the mean value of the strain and the slope gives the crystallite size. Fig. 7 shows the resulting graphs. Extracted data confirm a 6% increase in lattice strain and 19% change in crystallite size. These observations are indicative of potential retention of the removed substance within the nanodiamond structure, reinforcing the idea that an absorption path partakes in its decolorization process.

3.5.2. SEM analysis

To assess whether the observed structural changes resulted in morphologically observable alterations, SEM pictures of the nanodiamond pre- and post-decolorization were taken for comparison and are shown in Fig. 8. Prior to the

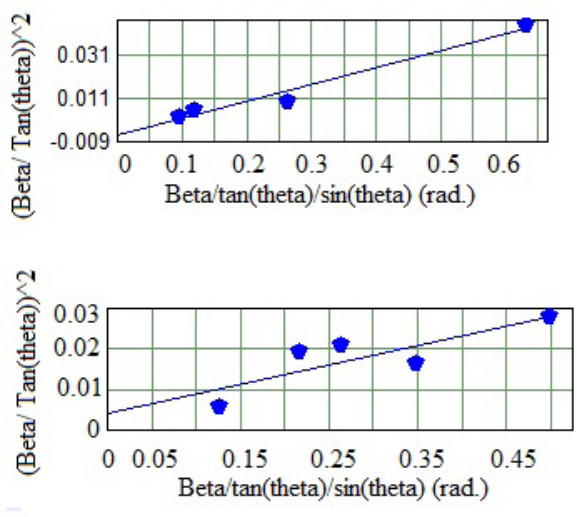

Fig. 7. Halder–Wagner resultant graphs for the pre- and post-nanodiamond treatment.

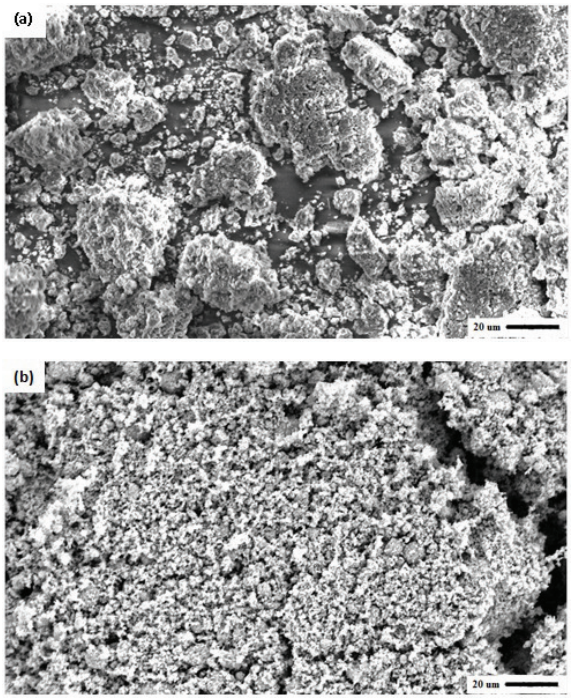

Fig. 8. SEM at 20 μm for nanodiamond—(a) before treatment; (b) after treatment (conditions: 0.1 g, HID xenon lamp).

sample being assessed in the SEM, it is placed in an oven to evaporate the liquid and leave the solid material behind. The dishes were then cooled, covered, and placed into a fume hood until analysis was performed.

As shown in the figure, the fluffy looking dispersed medium (Fig. 8(a)) has morphed into clumps of agglomerated material (Fig. 8(b)). The dispersion of the medium prior to decolorization suggests active binding sites. Having binding sites available allows a nanoparticle the capability of removing pollutants from the wastewater [36].

In Fig. 8(b), the SEM images confirm that there was some type of chemical interaction between the nanodiamond and the contaminant. This interaction having affected the surface characteristics of the catalyst such that even post-drying it remains in the clumped state.

4. Conclusions

This study looked to assess the viability of photocatalytic decolorization of acid blue–stained wastewater using nanodiamond. The findings would allow for an understanding of the routes of decolorization governing this carbon-based catalyst and validate their use as TiO_2 photocatalytic dopants. Decolorization was assessed using 3 catalysts namely, TiO_2, Fe–TiO_2, and nanodiamond. Feasibility was shown for all catalyst when all the light sources were used, and only the nanodiamond catalyst showed any effects when performed in the dark. The results performed in the light show that there is a small amount of photocatalytic response from the nanodiamond, and its effects are evident when small concentrations of it were used. The photocatalytic effect was minute in comparison with the absorption route confirmed in the dark reactor decolorization. This was confirmed using UV–Vis, XRD and SEM data showing both its effectiveness and retention. Considering its minor photocatalytic reaction, its highly efficient absorption behavior, and high rates of decolorization for multiple wavelength regions, nanodiamond would be a great candidate for a stand-alone wastewater-decolorizing agent as opposed to a dopant for a different catalyst. These observations are of importance to the aquatic sector that needs to gain good fundamental understanding of the governing parameters effecting treatment efficiency and how to improve them.

Acknowledgments

The authors would like to acknowledge West Texas A&M University and the Kilgore Research Grant program for providing the funds necessary to conduct this research (contract number WT16-046, Nano-Fluids for the Deactivation of Bacterial Bioagents). This work was also partly supported by the Ministry of Science and Technology of Taiwan under contract number: MOST 105-2119-M-259 -003 and MOST 105-2119-M-259 -002.

References

[1] T. Robinson, G. McMullan, R. Marchant, P. Nigam, Remediation of dyes in textile effluent: a critical review on current treatment technologies with a proposed alternative, Bioresour. Technol., 77 (2001) 247–255.
[2] G. Crini, Non-conventional low-cost adsorbents for dye removal: a review, Bioresour. Technol., 97 (2006) 1061–1085.
[3] C.Y. Ma, B.J. Dou, J.J. Li, J. Cheng, Q. Hu, Z.P. Hao, S.Z. Qiao, Catalytic oxidation of benzyl alcohol on Au or Au–Pd nanoparticles confined in mesoporous silica, Appl. Catal. B, 92 (2009) 202–208.
[4] G. Crini, Studies on adsorption of dyes on beta-cyclodextrin polymer, Bioresour. Technol., 90 (2003) 193–198.
[5] Q. Sun, L. Yang, The adsorption of basic dyes from aqueous solution on modified peat–resin particle, Water Res., 37 (2003) 1535–1544.
[6] C.C. Kaan, A.A. Aziz, S. Ibrahim, M. Matheswaran, P. Saravanan, Heterogeneous Photocatalytic Oxidation an Effective Tool for Wastewater Treatment – A Review, M. Kumarasamy, Ed., Studies on Water Management Issues, INTECH Open Access Publisher, 2012, pp. 219–236.

[7] A.O. Ibhadon, P. Fitzpatrick, Heterogeneous photocatalysis: recent advances and applications, Catalysts, 3 (2013) 189–218.
[8] M.A. Lazar, S. Varghese, S.S. Nair, Photocatalytic water treatment by titanium dioxide: recent updates, Catalysts, 2 (2012) 572–601.
[9] M. Pelaez M, N.T. Nolan, S.C. Pillai, M.K. Seery, P. Falaras, A.G. Kontos, P.S. Dunlop, A review on the visible light active titanium dioxide photocatalysts for environmental applications, Appl. Catal. B, 125 (2012) 331–349.
[10] R. Asahi, T. Morikawa, H. Irie, T. Ohwaki, Nitrogen-doped titanium dioxide as visible-light-sensitive photocatalyst: designs, developments, and prospects, Chem. Rev., 114 (2014) 9824–9852.
[11] Y.S. Ho, G. McKay, Sorption of dyes and copper ions onto biosorbents, Process Biochem., 38 (2003) 1047–1061.
[12] G.Z. Qu, J. Li, Y. Wu, G.F. Li, D. Li, Regeneration of acid orange 7-exhausted granular activated carbon with dielectric barrier discharge plasma, Chem. Eng. J., 146 (2009) 168–173.
[13] S.T. Akar, R. Uysal, Untreated clay with high adsorption capacity for effective removal of CI Acid Red 88 from aqueous solutions: batch and dynamic flow mode studies, Chem. Eng. J., 162 (2010) 591–598.
[14] S. Nayak, L.A. Lyon, Soft nanotechnology with soft nanoparticles, Ange. Chem., 44 (2005) 7686–7708.
[15] H. Meng, X.W. Chen, J.H. Wang, Ionic liquid templated porous nano-TiO_2 particles for the selective isolation of cytochrome c, Nanotechnol., 21 (2010) 385704.
[16] M.S. Mauter, M. Elimelech, Environmental applications of carbon-based nanomaterials, Environ. Sci. Technol., 42 (2008) 5843–5859.
[17] X. Wang, K. Maeda, X. Chen, K. Takanabe, K. Domen, Y. Hou, X. Fu, M. Antonietti, Polymer semiconductors for artificial photosynthesis: hydrogen evolution by mesoporous graphitic carbon nitride with visible light, J. Am. Chem. Soc., 131 (2009) 1680–1681.
[18] P. Qiu, C. Xu, H. Chen, F. Jiang, X. Wang, R. Lu, X. Zhang, One step synthesis of oxygen doped porous graphitic carbon nitride with remarkable improvement of photo-oxidation activity: role of oxygen on visible light photocatalytic activity, Appl. Catal. B, 206 (2017) 319–327.
[19] H. Lin, Y. Lu, J. Deng, S. Xie, X. Zhao, J. Yang, K. Zhang, Z. Han, H. Dai, Graphitic carbon nitride-supported iron oxides: high-performance photocatalysts for the visible-light-driven degradation of 4-nitrophenol, J. Photochem. Photobiol. A, 336 (2017) 105–114.
[20] H.D. Wang, Q. Yang, C.H. Niu, I. Badea, Adsorption of azo dye onto nanodiamond surface, Diamond Relat. Mater., 26 (2012) 1–6.
[21] C.C. Chen, E. Butler, M. Al Ahmad, Y.T. Hung, Y.P. Fu, Characterizations of TiO_2@ Mn-Zn ferrite powders for magnetic photocatalyst prepared from used alkaline batteries and waste steel pickling liquor, Mater. Res. Bull., 50 (2014) 178–182.
[22] E.B. Butler, C.C. Chen, Y.T. Hung, M.S. Al Ahmad, Y.P. Fu, Effect of Fe-doped TiO_2 photocatalysts on the degradation of acid orange 7, Integ. Ferroelectr., 168 (2016) 1–9.
[23] M. Shirzad-Siboni, S.J. Jafari, O. Giahi, I. Kim, S.M Lee, J.K. Yang, Removal of acid blue 113 and reactive black 5 dye from aqueous solutions by activated red mud, J. Ind. Eng. Chem., 20 (2014) 1432–1437.
[24] M. Saravanan, N.P. Sambhamurthy, M. Sivarajan, Treatment of acid blue 113 dye solution using iron electrocoagulation, Clean – Soil Air Water, 38 (2010) 565–571.
[25] L.Y. Lee, D.Z.B. Chin, X.J. Lee, N. Chemmangattuvalappil, S. Gan, Evaluation of *Abelmoschus esculentus* (lady's finger) seed as a novel biosorbent for the removal of Acid Blue 113 dye from aqueous solutions, Process Saf. Environ. Prot., 94 (2015) 329–338.
[26] A. Khataee, R. Darvishi Cheshmeh Soltani, Y. Hanifehpour, M. Safapour, Synthesis and characterization of dysprosium-doped ZnO nanoparticles for photocatalysis of a textile dye under visible light irradiation, Ind. Eng. Chem. Res., 53 (2014) 1924–1932.
[27] S.K. Kansal, M. Singh, D. Sud, Studies on photodegradation of two commercial dyes in aqueous phase using different photocatalysts, Hazard. Mater., 141 (2007) 581–590.
[28] L. Wang, W. Xiong, L. Yao, Z. Wang, Novel photocatalyic membrane reactor with TiO_2 nanotubes for azo dye wastewater treatment, MATEC Web Conf., 67 (2016) 06020.
[29] R.R. Dalbhanjan, N.S. Pande, B.S. Baerjee, S.P. Hinge, A.V. Mohood, P.R. Gogate, Degradation of patent blue V dye using modified photocatalytic reactor based on solar and UV irradiations, Desal. Water Treat., 57 (2016) 18217–18228.
[30] C. Galindo, C, P. Jacques, A. Kalt, Photooxidation of the phenylazonaphthol AO_{20} on TiO_2: kinetic and mechanistic investigations, Chemosphere, 45 (2001) 997–1005.
[31] S. Salthivel, B. Neppolian, M.V. Shankar, B. Arabindoo, M. Palanichamy, V. Murugesan, Solar photocatalytic degradation of azo dye: comparison of photo efficiency of ZnO & TiO_2, Sol. Energy Mater. Sol. Cells, 77 (2003) 65–82.
[32] I.K. Konstantinou, T.A. Albanis, TiO_2-assisted photocatalytic degradation of azo dyes in aqueous solution: kinetic and mechanistic investigation, Appl. Catal. B, 49 (2004) 1–14.
[33] M.N. Chong, Y.J. Cho, P.E. Poh, B. Jin. J, Evaluation of titanium dioxide photocatalytic technology for the treatment of reactive black 5 dye in synthetic and real greywater effluents, J. Clean. Prod., 89 (2015) 196–202.
[34] C.C. Wang, C.K. Lee, M.D. Lyu, L.C. Juang, Photocatalytic degradation of CI Basic Violet 10 using TiO_2 catalysts supported by Y zeolite: an investigation of the effects of operational parameters, Dyes Pigm., 76 (2008) 817–824.
[35] A. Garg, V.K. Sangal, P.K. Bajpai, Decolorization and degradation of reactive black 5 dye by photocatalysis: modeling, optimization and kinetic study, Desal. Water Treat., 57 (2016) 18003–18015.
[36] A. Khataee, R.D.C. Soltani, Y. Hanifehpour, M. Safarpour, H.G. Ranjbar, S.W. Joo, Synthesis and characterization of dysprosium-doped ZnO nanoparticles for photocatalysis of a textile dye under visible light irradiation, Ind. Eng. Chem. Res., 53 (2014) 1924–1932.